A Definitive Calibration Record for the Landsat-5 Thematic Mapper Anchored to the Landsat-7 Radiometric Scale

P.M. Teillet [1], D.L. Helder [2], T. Ruggles [2], R. Landry [1], F.J. Ahern [3], N.J. Higgs [4], J. Barsi [5], G. Chander [6], B.L. Markham [7], J.L. Barker [7], K.J. Thome [8], J.R. Schott [9], and F.D. Palluconi [10]

[1] *Canada Centre for Remote Sensing, 588 Booth Street, Ottawa, Ontario, Canada K1A 0Y7*

[2] *Electrical Engineering Department, South Dakota State University, Brookings, South Dakota, USA 57007*

[3] *TerreVista Earth Imaging, 441 Cormac Road, Cormac, Ontario Canada, K0J 1M0*

[4] *MacDonald Dettwiler and Associates Ltd, 13800 Commerce Parkway, Richmond, British Columbia, Canada, V6V 2J3*

[5] *Science Systems and Applications, Inc., NASA's Goddard Space Flight Center, Code 923, Greenbelt, Maryland, 20771*

[6] *Science Applications International Corporation, EROS Data Center, United States Geological Survey, Sioux Falls, South Dakota, 57198-0001*

[7] *NASA's Goddard Space Flight Center, Code 923, Greenbelt, Maryland, 20771*

[8] *Optical Sciences Center, University of Arizona, Tucson, Arizona, USA 85721-0094*

[9] *Center for Imaging Science, Rochester Institute of Technology, 54 Lomb Memorial Dr., Rochester, NY 14623*

[10] *Jet Propulsion Laboratory, Mail Station 183-501, 4800 Oak Grove Drive, Pasadena, CA 91109*

***Abstract**: A coordinated effort on the part of several agencies has led to the specification of a definitive radiometric calibration record for the Landsat-5 Thematic Mapper (TM) for its lifetime since launch in 1984. The time-dependent calibration record for Landsat-5 TM has been placed on the same radiometric scale as the Landsat-7 Enhanced Thematic Mapper Plus (ETM+). It has been implemented in National Landsat Archive Production Systems (NLAPS) in use in North America. The lifetime radiometric calibration record for Landsat will facilitate the examination of a continuous, near-global data set at 30-m scale that spans almost two decades. This paper documents the results of this collaborative effort and the specifications for the related calibration processing algorithms. The specifications include (1) anchoring of the Landsat-5 TM calibration record to the Landsat-7 ETM+ absolute radiometric calibration, (2) new time-dependent calibration processing equations and procedures applicable to raw Landsat-5 TM data and (3) algorithms for recalibration computations applicable to some of the existing processed data sets in the North American context.*

Introduction

The long and successful lifetime of the Landsat-5 Thematic Mapper (TM) has resulted in an almost unbroken archive of TM data covering most of the land areas of the Earth from 1984 to the present. Unfortunately, for a variety of reasons that are beyond the scope of this paper to review, the lifetime calibration record for Landsat-5 has not been properly maintained or documented over time. After the 1999 launch of Landsat-7 Enhanced Thematic Mapper Plus (ETM+), Landsat Program investigators placed the ETM+ and the Landsat-5 TM sensors on the same radiometric scale as of 1999 (Teillet et al., 2001). The remaining challenge has been to characterize the radiometric behaviour of the Landsat-5 TM over its lifetime going back to 1984. Though not reported here, similar efforts involving the Landsat-4 TM, launched in 1982, are also in progress by Landsat Program investigators. Collectively, these activities will allow the possibility of examining a continuous, near-global data set reaching back to 1982 with a view to monitoring global and regional land dynamics at a 30-m scale where both natural and anthropogenic disturbances can be assessed.

Radiometric calibration of Earth observation data from sensor systems such as Landsat is important for converting the data to physical units (spectral radiance and reflectance), comparing data from different scenes and different sensors over time periods ranging from days

to decades, and automating information extraction, particularly in the context of change detection and analysis. Radiometric calibration is simple in principle but difficult in practice. It is not realistic to expect that the calibration issues will be solved once and for all time. Data providers must retain scientists and/or engineers who monitor both the theory and implementation of radiometric calibration for all sensors in their "portfolio", maintain concise and accurate documentation, and provide prompt and authoritative responses to user inquiries regarding radiometric calibration.

In order to provide the best possible radiometric calibration of the Landsat data record for a wide variety of studies, especially those concerning sustainable development, a revised radiometric calibration of the Landsat-5 TM sensor for its entire mission has been developed and anchored to that of Landsat-7. The present paper documents the results of this collaborative effort and provides specifications for the related calibration algorithms. The specifications include (1) anchoring of the Landsat-5 TM calibration record to the Landsat-7 ETM+ absolute radiometric calibration, (2) new time-dependent calibration processing equations and procedures applicable to raw Landsat-5 TM data and (3) algorithms for recalibration computations applicable to some of the existing processed data sets in the North American context.

Cross-Calibration Between Landsat-5 and Landsat-7

Early in its mission, the Landsat-7 spacecraft was temporarily placed in a "tandem" orbit very close to that of the Landsat-5 spacecraft in order to facilitate the establishment of sensor calibration continuity between the Landsat-7 ETM+ and Landsat-5 TM sensors. The key period for the tandem-orbit configuration was June 1-4, 1999, during which hundreds of nearly-coincident matching scenes were recorded by both the Landsat-7 ETM+ and, in cooperation with Space Imaging / EOSAT and international ground stations, the Landsat-5 TM as well. A cross-calibration methodology, described elsewhere (Teillet et al., 2001), was formulated and implemented to use image pairs from the tandem-orbit configuration period to radiometrically calibrate the solar-reflective spectral bands of Landsat-5 TM with respect to the excellent radiometric performance of Landsat-7 ETM+. The radiometric calibration uncertainty for the ETM+ is considered to be ± 3 % (one sigma) (Barker et al., 2000). Markham et al. (2003) discuss on-orbit radiometric performance characterisations of the ETM+.

Amongst the matching scenes, only two are known to have coincident ground measurements associated with them. One in particular is the Railroad Valley Playa in Nevada (RVPN), which is used on a regular basis for sensor radiometric calibration based on surface measurements and which has a relatively stable and uniform surface compared to the majority of terrestrial surface types. Therefore, the RVPN results from the tandem-orbit-based cross-calibration analysis are considered to be the definitive set of Landsat-5 TM gain coefficients for June 1999 (Table 1). Tandem-orbit-based cross-calibration results from other image pairs (not shown) indicate a repeatability of the approach on the order of ± 2 %. For spectral bands 1-4, the estimated absolute uncertainty of this top-of-atmosphere radiance calibration is ± 3.6 % (one sigma), based on the root-sum-square of ± 3 % for ETM+ calibration and ± 2 % for the tandem-orbit-based cross-calibration. Uncertainty estimates have yet to be determined for spectral bands 5 and 7, but experience suggests that they will be approximately 50 % greater than the uncertainties in the first four spectral bands. Comparisons with results from independent vicarious calibration methods (Table 1) indicate that the tandem-orbit-based cross-calibration is in reasonable agreement with the independent results (within 2.5 % on average and no worse than within 4.4 %). A comparison between the 1999 and prelaunch TM gain coefficients is also included in Table 1. The large changes in gain in spectral bands 1-3 underscore the importance of post-launch calibration updates during the lifetime of the mission.

Table 1. Comparison of tandem-orbit-based (RVPN Xcal) and vicarious (RVPN UAZ) calibration results for Landsat-5 TM gain coefficients for the RVPN test site in June 1999. A comparison between RVPN Xcal and prelaunch gain coefficients is also included. Gains are in units of counts/(W/(m2 sr μm)).

Spectral Band	RVPN Xcal	RVPN UAZ	% Diff re Xcal		RVPN Xcal	Prelaunch Calibration	% Diff re Prelaunch
1	1.243	1.211	-2.60%		1.243	1.555	-20.0%
2	0.6561	0.627	-4.40%		0.6561	0.786	-16.5%
3	0.905	0.8953	-1.10%		0.905	1.02	-11.3%
4	1.082	1.111	+2.70%		1.082	1.082	0%
5	8.209	8.097	-1.37%		8.209	7.875	+4.24%
7	14.69	15.26	3.85%		14.69	14.77	-0.542%

Understanding TM Radiometry Over Time

Salient characteristics of the Landsat-5 TM have been documented elsewhere (cf. Markham et al., 1998, for example). For the purposes of this paper, it should be noted that the TM has an un-cooled primary focal plane (PFP) containing 16 silicon detectors per band for the four visible and near-infrared bands. Relay optics also transfer incident energy to the 92-Kelvin cold focal plane (CFP), which contains 16 InSb detectors for each of the short-wave infrared bands 5 and 7, plus four HgCdTe detectors for the thermal emissive band 6.

The TM sensors on both Landsat-4 and Landsat-5 incorporate an onboard radiometric calibration system called the Internal Calibrator (IC) (Mika, 1997). The IC has a shutter that oscillates back and forth directly in front of the PFP. The shutter includes optics to pipe light up from three internal calibrator lamps that are located near the base of the shutter flag. These lamps are normally continuously cycled through an eight-lamp state sequence over the course of a 24-second "scene" of data. The outputs from the lamps are monitored by unfiltered silicon photodiodes that sit behind a hole in each of the condenser mirrors in the lamp assemblies and the current to the lamps is controlled such that the outputs from the photodiodes are constant. The shutter oscillates in synchronization with the scan mirror such that, at the end of each scan, the shutter moves in front of the focal plane, blocks the Earth reflected light, and provides a dark zero signal as well as a beam of light from the internal calibrator lamps.

Image Artefacts and Within-Scene Relative Calibration

Analyses of the radiometric performance of the Landsat-4 and –5 TM sensors over the years have led to a detailed understanding of several image artefacts introduced by various characteristics of the actual sensors that differ from the ideal. Within-scene relative calibration algorithms have been developed and implemented in product generation systems around the world to remove most of these artefacts. Although the main artefacts have been well researched and documented, they are briefly summarized in Appendix 1 because several of them are mentioned in this paper in the context of radiometric processing steps.

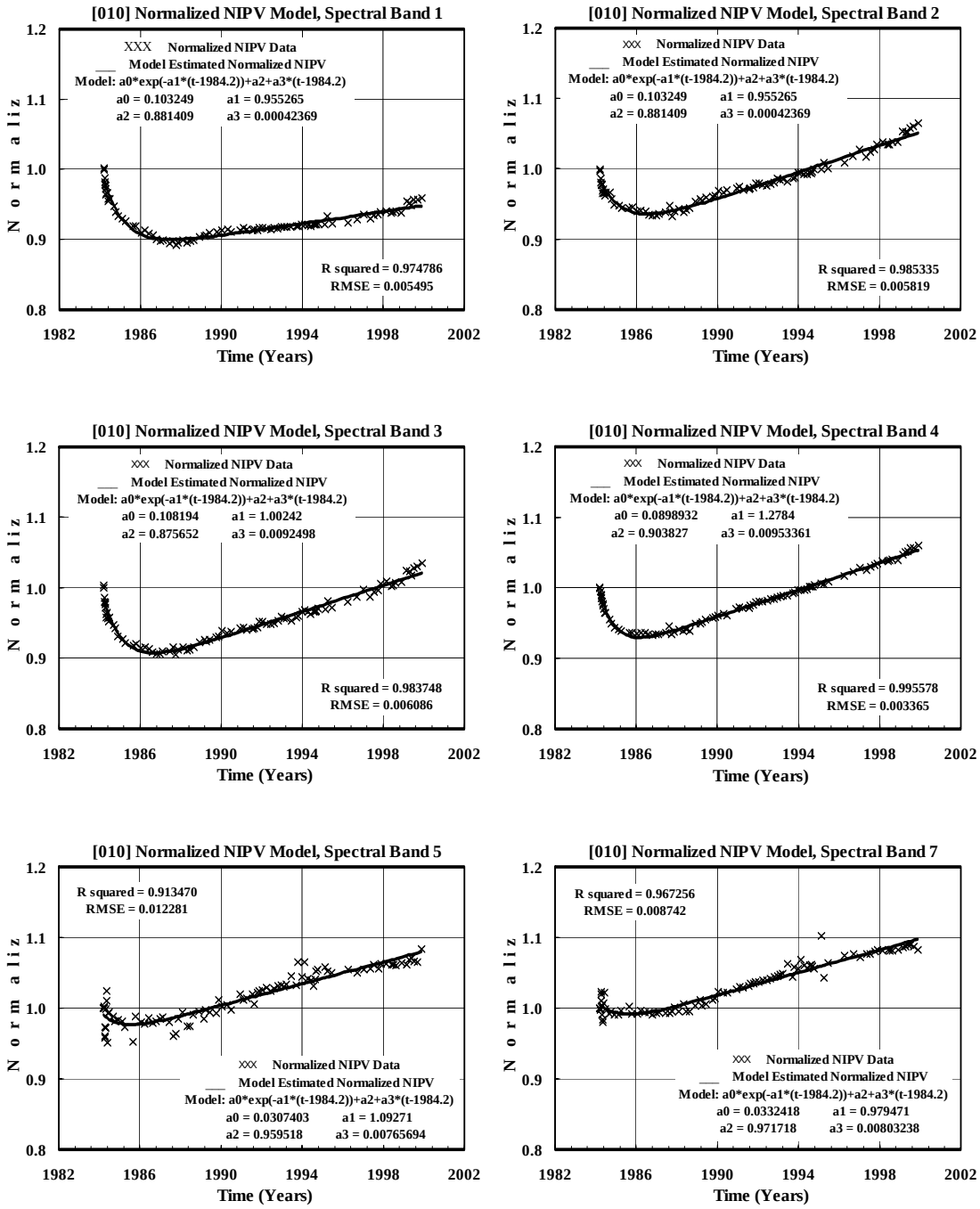

Figure 1: Lifetime plots of normalized net IC pulse values (NIPV) for lamp state [010] as a function of time since launch for the solar-reflective spectral bands of Landsat-5 TM.

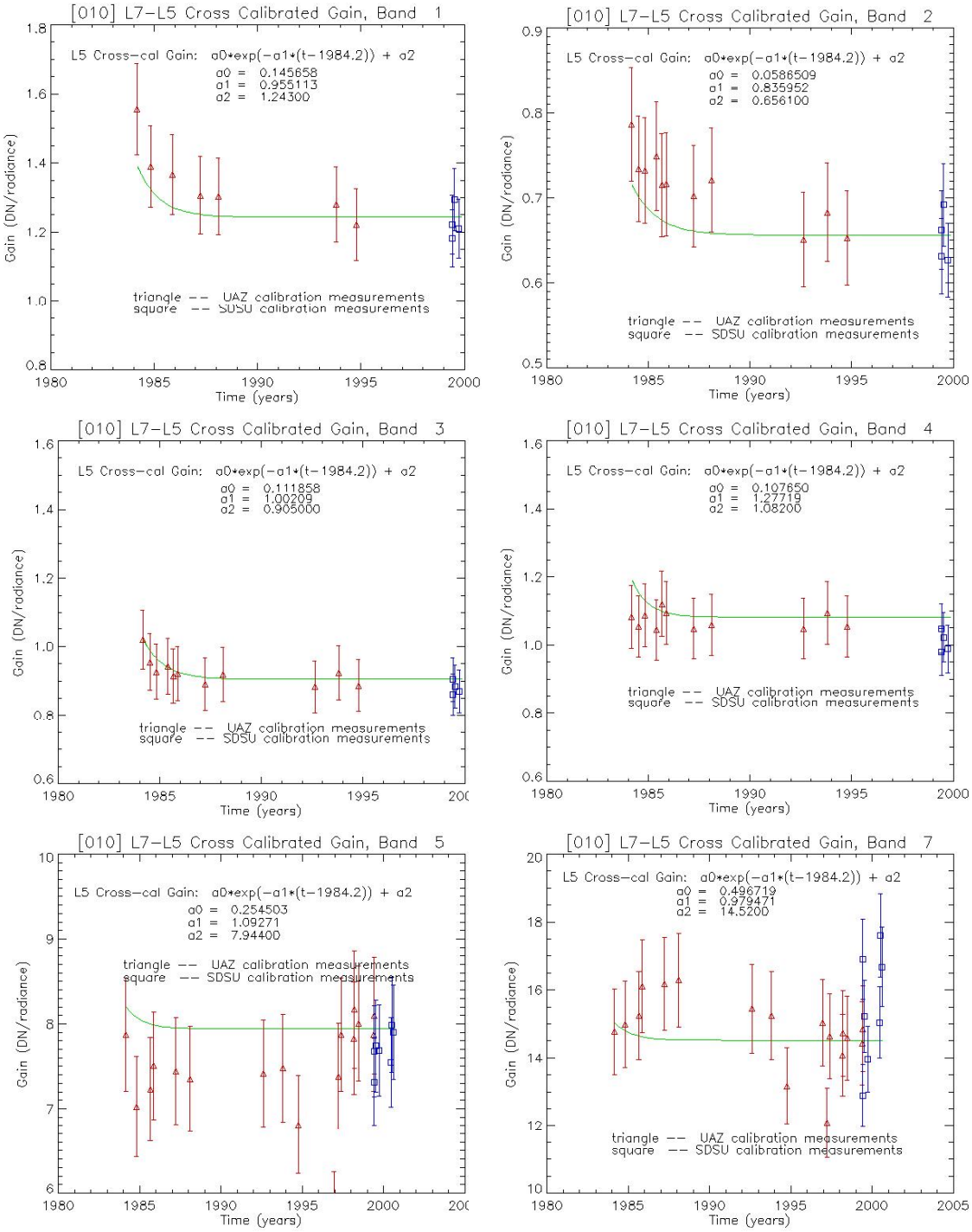

Figure 2: Lifetime gain plot for the solar reflective bands of Landsat-5 TM, tied to Landsat-7 cross-calibration measurements. DN = digital counts, radiance is in counts/(W/(m2 sr μm)), UAZ = University of Arizona and SDSU = South Dakota State University.

TM Internal Calibrator Trend Analysis (Solar-Reflective Bands)

Techniques have been developed to analyse data from the IC for the lifetime of the Landsat-5 TM (Helder, 1996; Helder et al. 1996; Markham et al., 1998; Helder et al., 1998a,b). The analysis indicates that only the IC pulses from reverse scans and lamp state #2 (010) should be used for characterizing the trend and for radiometric processing during TM product generation.

IC analysis results for the solar-reflective bands also indicate that the Landsat-5 TM lifetime radiometric trend takes a combined exponential plus linear form (shown for the solar-reflective spectral bands in Figure 1). The exponential part is deemed to be a true change in the TM (likely due to outgassing from the spectral filters during the first few years after launch) and the subsequent linear increase is considered to be a change in the IC system (likely due to changes in the lamp characteristics) rather than a true change in TM radiometric responsivity. Thus, in formulating the final temporal characterization (described in the next section), the linear trend is removed from the entire lifetime IC record based on the post-1988 fit.

A similar analysis is in progress by South Dakota State University and collaborators to characterize the Landsat-4 TM IC data.

Improved Radiometric Calibration for Raw Solar-Reflective Data From the Landsat-5 TM

The lifetime IC trend model for the Landsat-5 TM has been scaled to match the Landsat-7 ETM+ gain coefficient in each solar-reflective spectral band for June 1, 1999, as determined by the tandem-based cross-calibration for the RVPN test site. The resulting curves (Figure 2) are generally consistent with independent vicarious calibration results obtained by the University of Arizona over the years (Thome et al., 1997**)** and by South Dakota State University in 1999 (Black et al., 2003). Thus, the time-dependent equations for Landsat-5 TM gain, $G_{new}(t)$, applicable to raw data, take the form

$$G_{new}(t) = a0*\exp(-a1*(t - 1984.2)) + a2 \quad , \quad (1)$$

where the time t is in decimal years, the coefficients a0, a1, and a2 are given in Table 2, and 1984.2 refers to the launch date of Landsat-5. Note that the TM gain coefficients in the solar-reflective bands have been constant to within the accuracy of the vicarious calibration methodology since approximately 1987.

Due to the periodic build up of ice during outgassing cycles (Appendix 1), there is an additional ± 2-3 % uncertainty in bands 5 and 7 of any given TM product. A thin-film model has been developed to correct for most of this effect (Liew and Helder, 2003). The oscillatory nature of this model is such that the $G_{new}(t)$ for these bands will be better specified in terms of day-specific look-up tables (LUTs) for bands 5 and 7. Hence, for practical purposes in the processing, LUTs will be used for $G_{new}(t)$ for all six solar-reflective bands.

Table 2. Coefficients for time-dependent characterization of Landsat-5 TM lifetime gain based on IC trend analysis, anchored to Landsat-7 ETM+ via cross-calibration using the tandem-orbit image pair for RVPN in 1999. Coefficients a0 and a2 are in units of counts/(W/(m2 sr μm)) and the a1 coefficients are dimensionless.

Spectral Band	a0	a1	a2
1	0.1457	0.9551	1.243
2	0.05865	0.8360	0.6561
3	0.1119	1.002	0.9050
4	0.1077	1.277	1.0820
5	0.2545	1.093	7.944
7	0.4967	0.9795	14.52

Recommendations for Radiometric Calibration Processing of Raw Archival Data for the Solar-Reflective Bands

The operational radiometric processing of raw TM data involves many steps. While it is beyond the scope of this paper to describe the details, the following sequence of steps outlines how the new lifetime gain equation should fit into the radiometric calibration processing of raw archival data for the solar-reflective bands. Computationally, some of the steps will be wrapped up together.

- Correction for scan-correlated shifts via bias subtraction on a scan-specific basis.
- Correction for the memory effect in spectral bands 1-4.

- No correction for the coherent noise effect (typically on the order of 0.15 DN or less).
- Correction for the temperature effect based on IC pulses from reverse scans and lamp state #2 (010).
- Correction for cold focal plane filming due to outgassing based on IC pulses from reverse scans and lamp state #2 (010).
- Correction for relative detector gain differences using lifetime scene statistics and normalization to band average.
- Absolute radiometric calibration using the LUTs for $G_{new}(t)$.
- Bias processing (unchanged) based on line-specific dark current readings.
- Output scaling (unchanged) to allow use of time-invariant calibration coefficients by users.

Radiometric Recalibration Algorithm for Existing Data Products

Over the lifetime of the Landsat-5 TM, significant investments have been made to collect radiometrically calibrated TM data over large geographic areas in a variety of application contexts. Hence, there is considerable interest in the possibility of creating and providing an algorithm to allow users to recalibrate these Level-1 image data to take advantage of the new lifetime TM calibration record without having to repurchase their data products if possible.

There have been three US processing systems to convert raw satellite digital numbers (DN) to calibrated radiances for Landsat-5. The initial processing system for Landsat-5 was called the TM Image Processing System (TIPS), used first by NOAA and subsequently by a private company, Earth Observation Satellite Company (EOSAT, now known as Space Imaging) when it took over the operation of Landsat-5 in 1985. In October 1991, EOSAT updated its processing system to the Enhanced Image Processing System (EIPS). In July 2001, Landsat-5 operation and its entire image archives were turned back over to the US government to be operated by the US Geological Survey's (USGS) EROS Data Center (EDC), Sioux Falls, South Dakota. So far, the USGS archive for Landsat-5 has always been processed with the National Landsat Archive Production System (NLAPS), built by MacDonald Dettwiler and Associates (MDA) of Richmond, B.C.

MDA has built all of the Landsat production systems used in Canada over the years, in collaboration with the Canada Centre for Remote Sensing (CCRS), as well as a significant

proportion of the Landsat processing systems used around the world. The first MDA Landsat TM processing system was the TM Bulk Processing System (TMBPS), built in the early 1980s. TMBPS was operated by MDA in Richmond, B.C. until the Multi-Observation Satellite Image Correction System (MOSAICS) was developed and delivered to the Prince Albert Satellite Station (PASS) in January 1987. MOSAICS was operated by CCRS at PASS until April 1990 when it was moved to the private company Radarsat International (RSI) in Richmond, B.C. In September 1993, RSI replaced MOSAICS with the Geocoded Image Correction System (GICS), also developed by MDA. RSI used GICS to produce TM products until April 2000, when production switched over to the Product Generation System (PGS), an MDA-supplied processor for Landsat-7 and Landsat-5.

The TM image products generated by all of the aforementioned systems have been or could have been bias corrected, de-striped based on scene statistics, and calibrated using the onboard IC system. In North America, the vast majority of calibrated Landsat-5 TM images were processed on either NLAPS or TIPS.

User Recalibration Equations

In the original product generation process, the uncalibrated Q values (in counts) have been converted to calibrated Q values (Q_{cal}) by applying the calibration processing parameters α and β, described in Appendix 2. Recalibration consists of finding and using the original α and β and applying the new calibration coefficients, $G_{new}(t)$.

The equation to convert from the old calibrated Q values, $Q_{cal,old}$, to the revised calibrated Q values, $Q_{cal,new}$, is (Appendix 2):

$$Q_{cal,new} = \frac{G}{G_{new}(t)}[\alpha_{ref} Q_{cal,old} + \beta_{ref} - 3] + Q_o \quad . \qquad (2)$$

G and Q_o are the calibrated gain and offset, respectively, as described in Appendix 2. Thus, the key to recalibration is knowledge of the original α_{ref} and β_{ref} coefficients used to generate the product, which were nominally based on scene statistics and the IC pulse data in the original processing.

The original calibration processing coefficients can be obtained using one of three approaches:

1. The easiest way to obtain values for α_{ref} and β_{ref} is from the Radiometric Quality Assessment Work Order Report that accompanied the product in hard copy or as a computer file when it was delivered to the user.

2. α_{ref} and β_{ref} can be obtained from the radiometric ancillary record of the leader file for the LGSOWG format (often called CCT format), where LGSOWG refers to the Landsat Ground Station Owners Working Group.

3. If the user has data with no history of its radiometric processing, the recalibration can be performed using the band average discrete values derived over the lifetime of the Landsat-5 TM (Appendix 2). This will not produce the same accuracy as the use of the two aforementioned approaches.

It is important to note that the values of α_{ref} and β_{ref} are obtained from the forward scans on all MOSAICS and GICS products, but products from the PGS use the reverse scans for all data acquired during and after 1995. This change was implemented to overcome problems in acquiring proper forward scan data from the IC because of bumper wear on the Landsat-5 TM scan mirror, which has resulted in the lengthening of scans with increasing age of the instrument.

If the user wishes to calculate revised at-sensor radiance L^*_{new} directly from the original Q_{cal} data, the equation is as follows (Appendix 2):

$$L^*_{new} = \frac{\alpha_{ref} Q_{cal,old} + \beta_{ref} - 3}{G_{new}(t)} \quad . \qquad (3)$$

The user's circumstances will dictate whether it is more appropriate to compute $Q_{cal,new}$ or L^*_{new} directly.

In any case, it is imperative that the user record and retain a record of the change in calibration together with the recalibrated data. It is only through careful and permanent record keeping that the possibility of a future researcher using the recalibrated data with the inappropriate calibration coefficients can be avoided.

Radiometric Calibration for Thermal Infrared Data From the Landsat-5 TM

An assessment of the Landsat-5 thermal band calibration has been carried out by Barsi et al. (2003). Their work is based on recent and historical analyses and includes a cross-calibration with respect to the Landsat-7 ETM+. The compiled results indicate that the Landsat-5 TM has not deteriorated as much as some papers in the literature have suggested. The results indicate an offset error of +0.096 ± 0.026 W/(m2 sr μm), or -0.71 ± 0.2 K at 300 K over the lifetime of the instrument, with Landsat-5 TM data being colder than the ground reference data. There is no suggestion of any trend with time. Thus, users should retrospectively subtract 0.71 K from existing temperature data sets derived from Landsat-5 TM band 6. It is recommended that a correction for this apparent calibration offset error be implemented in Landsat-5 product generation systems at the earliest opportunity.

Concluding Remarks

The excellent radiometric performance of the Landsat-7 ETM+ together with a tandem-orbit-based cross-calibration in the solar-reflective bands have made it possible to put the Landsat-5 TM and Landsat-7 ETM+ on the same radiometric scale. Detailed analyses of lifetime TM calibration data, undertaken by South Dakota State University and collaborators, have led to the development of a definitive absolute radiometric calibration record for the solar reflective bands for the lifetime of the Landsat-5 TM. It has been implemented in the form of a look up table (LUT) in NLAPS for products generated at the EROS Data Center as of May 5, 2003 and on other NLAPS systems elsewhere thereafter.

With respect to the thermal band, recent results from Landsat-5 TM vicarious calibration efforts show an offset of -0.7 K over the lifetime of the instrument. A correction to the Landsat-5 processing has been implemented accordingly. These results indicate that historical calibration efforts were detecting errors in processing systems rather than changes in the instrument.

Although accuracy assessments will be done in due course, it is anticipated that lifetime Landsat-5 TM radiometric calibration can be established to approximately the following

absolute accuracies (with higher accuracies in bands 1-4 and greater uncertainties in bands 5 and 7):

±5%-15% (one sigma) with no calibration updates;

±5%-10% (one sigma) with the application of user recalibration equations to existing products originally obtained from North American processing systems;

± 3%-5% (one sigma) with reprocessing of raw archival data on processing systems in North America with lifetime calibration updates.

± 2 K (one sigma) for band 6, with the expectation that this will be improved in the near future.

It is remarkable that the Landsat-5 TM has continued to perform so well for a time far exceeding its original design life. Full implementation of the processing changes recommended in this paper should lead to superior Landsat 5 TM data products, comparable in radiometric quality to Landsat-7 ETM+ data, thus providing the basis for continued long-term studies of the Earth's land surfaces.

It is expected that a similar analysis can be completed for the Landsat-4 TM, thus extending the 30-m Landsat coverage back to 1982. The merits and feasibility of placing Multispectral Scanners (MSS) data from the first five Landsat missions, extending back to 1972, on the same radiometric scale need to be assessed before undertaking any MSS recalibration effort. It is doubtful that the radiometric calibration accuracy of MSS data could be improved significantly.

Acknowledgements

The work presented in this paper has been supported by the Landsat Project Science Office, NASA's Goddard Space Flight Center, as well as by NASA grant NAG5-2448 to the University of Arizona and NASA grants NAG5-3540 and NAG5-3445 to South Dakota State University. The authors are also pleased to acknowledge the generous contributions of time and information by Brian Robertson, Shu Cheung Tang and Pat Campbell of Macdonald Dettwiler and Associates, Don Herriot of Radarsat International, and Esad Micijevic of South Dakota State University.

References

Ahern, F.J., and J. Murphy, l979. Radiometric Calibration and Correction of LANDSAT l, 2, and 3 MSS Data, Canada Centre for Remote Sensing Research Report 78-4, Canada Centre for Remote Sensing, 588 Booth Street, Ottawa, Ontario, K1A 0Y7, Canada.

Barker, J. L, and F. J. Gunther, 1983. "Landsat-4 Sensor Performance", Proceedings of the Pecora VIII Symposium, Satellite Land Remote Sensing Advancements for the Eighties, Sioux Fall, South Dakota, October 4 – 7, pp 46 – 74.

Barker, J.L., S.K. Dolan, P.A. Sabelhaus, D.L. Williams, J.R. Irons, B.L. Markham, J.T. Bolek, S.S. Scott, R.J. Thompson, J.J. Rapp, T.J. Arvidson, J.F. Kane, and J.C. Storey, 2000. "Landsat-7 Mission and Early Results", Proceedings of the SPIE Conference on Sensors, Systems, and Next-Generation Satellites V, SPIE Volume 3870, Florence, Italy, pp. 299-311.

Barsi, J.A., J. R. Schott, F. D. Palluconi, D. L. Helder, S. J. Hook, B. L. Markham, G. Chander, and E. M. O'Donnell, 2003. "Landsat TM and ETM+ Thermal Band Calibration", Canadian Journal of Remote Sensing, 29(2): 141-153.

Black, S.E., D.L. Helder, and S.J. Schiller, 2003. "Irradiance-Based Cross Calibration of Landsat-5 and Landsat-7 Thematic Mapper Sensors", International Journal of Remote Sensing, 24(2): 287-304**.**

Helder, D.L., 1996. "A Radiometric Calibration Archive for Landsat TM", Proceedings of the SPIE Conference on Algorithms for Multispectral and Hyperspectral Imagery", SPIE Volume 2758, Orlando, Florida, pp. 273-284.

Helder, D.L., J. Barker, W. Boncyk, and B.L. Markham, 1996. "Short Term Calibration of Landsat TM: Recent Findings and Suggested Techniques", Proceedings of 1996 International Geoscience and Remote Sensing Symposium (IGARSS'96), Lincoln, Nebraska, pp. 1286-1289.

Helder, D., W. Boncyk, and R. Morfitt, 1997. "Landsat TM Memory Effect Characterization and Correction", Canadian Journal of Remote Sensing, 23(4): 299-308.

Helder, D.L., W. Boncyk, and R. Morfitt, 1998a. "Absolute Calibration of the Landsat Thematic Mapper Using the Internal Calibrator", Proceedings of 1998 International Geoscience and Remote Sensing Symposium (IGARSS'98), Seattle, Washington, pp. 2716-2718.

Helder, D.L., W. Boncyk, and R. Morfitt, 1998b. "Landsat TM Memory Effect Characterization and Correction", Canadian Journal of Remote Sensing, 23(4), 299-301.

Kieffer, H. H., D. A. Cook, E. M. Eliason, and P. T. Eliason, 1985. "Intraband radiometric performance of the Landsat Thematic Mapper", Photogrammetric Engineering and Remote Sensing, 51:1391-1394.

Liew, S.-W., and D.L. Helder, 2003. "Landsat-5 Thematic Mapper Cold Focal Plane Characterization", International Journal of Remote Sensing, 24(2): 249-263.

Markham, B.L., J.L. Barker, E. Kaita, J. Seiferth, and R. Morfitt, 2003. "On-Orbit Performance of the Landsat-7 ETM+ Radiometric Calibrators", International Journal of Remote Sensing, 24(2): 265-285.

Markham, B.L., and J.L. Barker, 1986. "Landsat MSS and TM Post-Calibration Dynamic Ranges, Exoatmospheric Reflectances, and At-Satellite Temperatures", Landsat Technical Notes, Earth Observation Satellite Company (EOSAT), Lanham, Maryland**,** Volume 1, No.1, August 1986, pp. 3-8.

Markham, B.L., J.C. Seiferth, J. Smid, and J.L. Barker, 1998. "Lifetime Responsivity Behavior of the Landsat-5 Thematic Mapper", Proceedings of SPIE Conference 3427, San Diego, California, pp. 420-431.

Metzler, M.D., and W.A. Malila, 1983a. "Radiometric Characterization of Thematic Mapper Full-frame Imagery", Proceedings of the SPSE/ASP Conference on Techniques for Extraction of Information from Remotely Sensed Images, Rochester, New York, **pages?**.

Metzler, M.D., and W.A. Malila, 1983b. "Scan-angle and Detector Effects in Thematic Mapper Radiometry", Proceedings of the Landsat-4 Science Characterization Early Results Symposium, January 1983, Vol. II, NASA Conference Publication 2355, pp. 421-441.

Metzler, M.D., and W.A. Malila, 1985. "Characterization and Comparison of Landsat-4 and Landsat-5 Thematic Mapper Data", Photogrammetric Engineering and Remote Sensing, 51:1315 – 1330.

Mika, A.M. 1997. "Three Decades of Landsat Instruments", Photogrammetric Engineering and Remote Sensing, 63(7):839-852.

Murphy, J.M, 1986. "Within-Scene Radiometric Correction of Landsat Thematic Mapper Data in Canadian Production Systems", Proceedings of the Earth Remote Sensing Using Landsat

Thematic Mapper and SPOT Sensor Systems, SPIE Volume 660, Innsbruck, Austria, April 15 – 17, pp. 25-31.

Murphy, J.M., 1984. Radiometric Correction of Landsat Thematic Mapper Data, CCRS Digital Methods Division Technical Memorandum DMD-TM#84-368, Canada Centre for Remote Sensing, 588 Booth Street, Ottawa, Ontario, K1A 0Y7, Canada.

Srinivasan, R., M. Cannon, and J. White, 1988. "Landsat Data Destriping Using Power Spectral Filtering", Optical Engineering, 27(11): 939-943.

Teillet, P.M., J.L. Barker, B.L. Markham, R.R Irish, G. Fedosejevs, and J.C. Storey, 2001. "Radiometric Cross-Calibration of the Landsat-7 ETM+ and Landsat-5 TM Sensors Based on Tandem Data Sets", Remote Sensing of Environment, 78(1-2): 39-54.

Thome, K., B. Markham, J. Barker, P. Slater, and S. Biggar, 1997. "Radiometric Calibration of Landsat", Photogrammetric Engineering and Remote Sensing, 63(7):853-858.

Appendix 1. Image Artefacts and Within-Scene Relative Calibration

Striping

Striping consists of stripes in the image resulting from differences in gain and bias of the individual detector elements. Striping has been the most severe of the radiometric artefacts of all of the Landsat multispectral scanners, beginning with the Multispectral Scanner (MSS) on Landsat-1 in 1972. A destriping algorithm was developed at CCRS for the MSS on Landsat 1 (Ahern and Murphy, 1979) and was improved and adapted to the TM sensor by Murphy (1984). This algorithm has proven very reliable and has been incorporated into the TMBPS, MOSAICS, GICS, LPGS, and PGS systems. The algorithm uses scene-based histogram equalization to provide a relative radiometric calibration in each solar-reflective band to reduce "striping". The destriping algorithm works by determining the bias and gain of each of the individual detector elements relative to a reference detector, and then equalizing the bias and gain of each of the individual detector elements to the bias and gain of the reference detector. In most US implementations, the reference detector is really a pseudo-detector with gain and bias calculated as the arithmetic mean of the gains and biases of the actual individual detector elements. In Canada, a single detector has been chosen as the reference detector for each spectral band.

Scan-Correlated Shift

Scan-correlated shift is a sudden change in detector bias that occurs in the time interval between scans. The amount of change is typically quite small, on the order of one digital count or less. All detectors change at the same time, but with different amplitudes. Since all detectors change simultaneously, the effect can be seen in the data as bands (sixteen lines wide) that are of slightly different intensity. The effect occurs randomly, across multiple scans, and without significant evidence of periodic structure. It arises in the TM and ETM+ because onboard circuitry automatically restores the bias to a nominal value after each observation of the black shutter at the end of each scan line. This so-called "DC restore" prevents the bias from drifting too far from its nominal value. However, it also causes the bias to change slightly between a

given scan line and the next. An accurate characterization of the bias level for each scan is made by the image production system from the "before-DC-restore" portion of the signal. This characterization is used to correct the bias of the individual detector elements on a scan-by-scan basis, for both the image portion of the data and for the internal calibrator portion, which is used to measure the intensity of the signal from the calibration lamps. This effect changes little over time and has no periodicity.

Memory Effect

The Landsat TM memory effect results from relatively short-term changes in gain that occur when one or more detector elements are overloaded by viewing a very bright target and it has been thoroughly investigated and reported (Barker and Gunther, 1983; Kiefer et al., 1985; Murphy, 1986; Srinivasan et al., 1988; Helder et al., 1997). The memory effect produces light and dark bands in the imagery and is most obvious in homogeneous regions following a sudden transition in intensity, such as at a cloud/land boundary. It is also known by other names, including "banding", "bright target recovery", "bright target saturation", "scan-to-scan striping", and "radiometric hysteresis". Every image pixel is affected and the magnitude of the effect can reach as high as 2 digital counts. The memory effect has not been observed in bands 5, 6, and 7, which are in the cold focal plane and use preamplifiers that are designed differently compared to those used in TM bands 1 to 4. Helder et al. (1997) trace the memory effect to the pre-amplifiers that amplify the analog signal from each individual detector element. Following saturation by a bright target, the output of the pre-amplifier undershoots the desired level and recovers exponentially with a time constant of 10 milliseconds, which corresponds to 1040 pixels.

Correction of the memory effect requires convolution of the digital image signal data with the inverse of the memory effect pulse response function. Because of the long time constant, this convolution is very computationally demanding and was beyond the computational power of the systems available in the 1980s. However, a correction was implemented on the PGS. Correction of the memory effect became a default correction on data produced on PGS by RSI beginning on Apri1 1, 2001. Because correction requires full data sets, i.e., image data as well as IC pulse and shutter data, it is not applicable to non-archival data sets for which the non-image data have not been kept.

Coherent Noise

Coherent noise consists of low levels of electronic noise picked up from various electronic components on the sensor and spacecraft. Because of the very high sensitivity of the TM image amplifiers, it is difficult to completely eliminate low levels of electronic noise that can affect the data. Coastal water applications are the most affected potentially. A description and general characterization of the coherent noise have been reported by Metzler and Malila (1983a,b, 1985). The noise consists of several different components with varying amplitudes, frequencies and phases that may be present or absent depending upon which particular spacecraft circuits are operating at the time of image acquisition. The characterization needed for correction would be very difficult to perform on a scene-by-scene basis because the coherent noise is quite small compared to actual image data. Fortunately, the amplitude of the noise introduced by coherent noise is small, typically 0.25 counts or less for the Landsat-5 TM (Helder et al., 1997) and even smaller for ETM+. Coherent noise is not corrected in TM and ETM+ production systems.

Oscillations Due to Cold Focal Plane Icing

The detectors for bands 5, 6, and 7 are located in the Cold Focal Plane (CFP). To minimize thermal noise and allow adequate detection of scene energy, the CFP has its temperature maintained between 95 and105 K through the use of a radiative cooler. During an out-gassing cycle, oscillations have been observed in the band 5 and 7 gains over time. These oscillations are believed to be due to the build up of an ice film on the window separating the cooled and warm portions of the optical path. The peak-to-peak amplitude of the oscillations is approximately 3 % to 5 % and is detected and corrected through observations of Internal Calibrator data. Correction of the gain oscillations is based on a thin-film interference model approach developed at South Dakota State University (Liew and Helder, 2003). The model is based on an analysis of closely sampled sets of detector responses from the TM's lifetime. The approach relates detector behaviour to both the accumulated ice thickness since the previous outgassing cycle and the current growth rate of the ice film.

Appendix 2: Theoretical Formulation and Derivation of Key Equations

General Theory

This appendix presents the theoretical formulation of the radiometric calibration process and the derivation of key equations. Note that each spectral band is treated independently, so the variables presented here will take on different values for each spectral band.

The detectors in the Landsat instruments are assumed to exhibit linear response to scene radiance and to the Internal Calibrator lamp radiances. The detector responses are quantized into 8-bit numbers between 0 and 255. The recorded quantized signal level, Q (in counts), is related to the (spectral) radiance of a pixel, L*, by the following equation:

$$Q = G_d L^* + Q_{db}, \qquad (1)$$

where G_d (in counts per unit radiance) represents the gain of detector d (more formally known as responsivity), Q_{db} (in counts) represents the bias of detector d, and the asterisk indicates that the radiance is an at-sensor, or top-of-the-atmosphere (TOA), radiance.

The goal of sensor radiometric calibration is to establish and understand the relationship given by equation (1). However, that relationship typically changes over time, particularly during the first few years on orbit. Therefore, the generation of Landsat image data products for users has always been such that these changes are transparent to users and that the users can use time-invariant coefficients to compute radiance from a radiometrically-calibrated product. Accordingly, the objective of radiometric calibration processing is to transform the data actually recorded, represented by Q, to calibrated signal levels, represented by Q_{cal}. Thus, the Landsat image user can always compute at-sensor radiance, L*, from Qcal using a time-invariant relationship:

$$Q_{cal} = GL^* + Q_o \quad , \qquad (2)$$

where Q_{cal} is the calibrated signal level (in counts), G is the calibrated gain (in counts per unit radiance), and Q_o is the calibrated offset (in counts). The radiometrically-calibrated product consists of Q_{cal} in so-called calibrated counts. The parameters G and Q_o are defined prior to launch by the sensor calibration team and are intended to be time-invariant for ease of use.

Since detector-to-detector differences are removed as part of the calibration process, G and Q_o are also detector independent. However, the relationship between radiance and the calibrated signal is different for each spectral band, so separate values of G and Q_o are specified for each band.

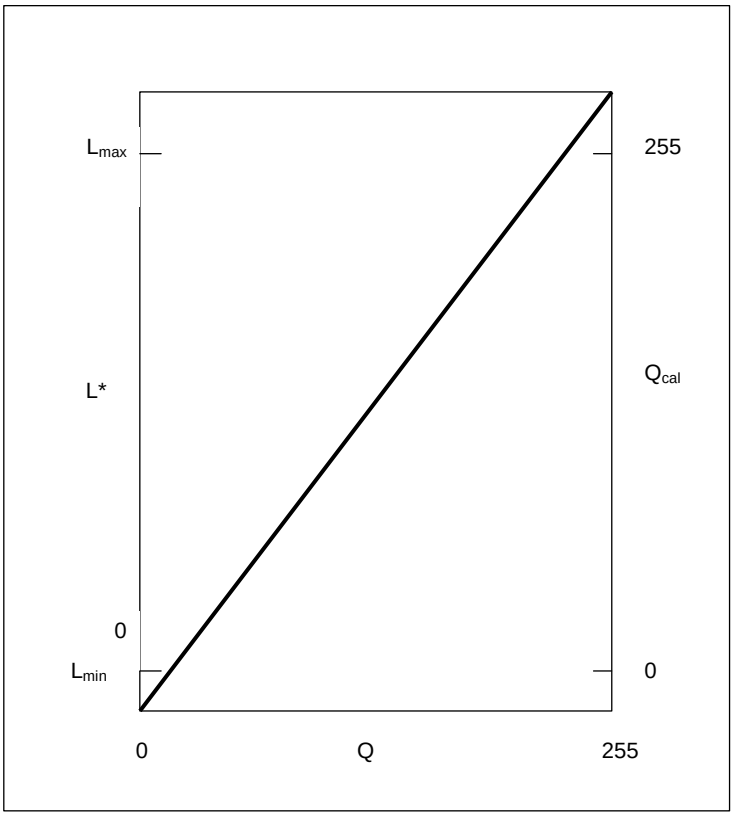

Figure A1: Schematic representation of the linear relationship between raw data (Q), observed radiance (L*), and calibrated data (Q_{cal}).

The linear relationships in equations (1) and (2) are shown schematically in Figure A1. The slope and intercept of the calibration relationship are determined through the establishment of the lower and upper ends of the radiance scale, which are designated L_{min} and L_{max}, respectively. For calibrated data, $Q_{cal} = Q_{cal,min}$ corresponds to $L^* = L_{min}$, and $Q_{cal} = Q_{cal,max}$ corresponds to $L^* = L_{max}$, as shown in Figure A1. Most Landsat TM and ETM+ production systems follow the convention of assigning $Q_{cal,min} = 0$ and $Q_{cal,max} = 255$. However, the Landsat Product Generation System operated by the US Geological Survey's EROS Data Center reserves $Q_{cal} = 0$ for zero-fill and follows the convention $Q_{cal,min} = 1$ for Landsat-7 ETM+ products.

Solving equation (1) for L* and substituting into equation (2) provides an equation to transform uncalibrated data, Q, into calibrated data, Q_{cal}.

$$Q_{cal} = \frac{G}{G_d}[Q - Q_{db}] + Q_o \quad . \qquad (3)$$

Hence, the challenge of calibration processing in product generation systems is to find reliable means to determine the time-dependent calibration parameters G_d and Q_{db}.

With a radiometrically-calibrated product in hand, the user has all the necessary parameters to compute at-sensor radiance (based on equation (2)):

$$L^* = \frac{1}{G}\left[Q_{cal} - Q_o\right] \quad . \qquad (4)$$

Nominally, users are also provided with time-invariant L_{min} and L_{max} for each spectral band, which implies that G and Q_o can also be obtained as follows:

$$G = [Q_{cal,\max} - Q_{cal,\min}] \div [L_{\max} - L_{\min}] \quad , \qquad (5)$$

$$Q_o = -G\, L_{\min} \quad . \qquad (6)$$

Unfortunately, most Landsat product generation systems adopted a formulation that differs from the proper one given by equation (4) in that the user calibration equation is written as $L^* = Q_{cal}\, G + Q_o$, in which case G is in radiance per unit count and Q_o is in radiance. A common form of this equation is (Markham and Barker, 1986) $L^* = A_1\, G + A_o$, where A_1 is the inverse of equation (5) and A_0 is L_{min}. Utilization of this formulation should be discouraged and those product generation systems that use it should make a special effort to guide users in this respect.

Formulation for ETM+ Data

For Landsat-7 ETM+ data, the calibration process is very straightforward. Q_{db} is obtained for every scan line when the sensor views the dark shutter. G_d is determined by the sensor calibration team from studies of prelaunch and post-launch calibration data. The currently accepted best value for G_d is made available to users and organizations that produce ETM+ data products in a Calibration Parameter File (CPF) updated quarterly and posted on the Landsat mission website. Equation (3) is used in the product generation system to convert raw data, Q, to calibrated data, Q_{cal}.

If the need arises to recalibrate ETM+ data, "old" and "new" versions of equation (3) are introduced to indicate the original calibration and the revised calibration:

$$Q_{cal,old} = \frac{G}{G_{d,old}}[Q - Q_{db}] + Q_o \quad , \qquad (7)$$

$$Q_{cal,new} = \frac{G}{G_{d,new}}[Q - Q_{db}] + Q_o \quad . \qquad (8)$$

It is expected that there will be no change in the method to determine Q_{db}, since it has proven very reliable, so the factor $[Q - Q_{db}]$ remains unchanged. Solution of equation (4) for $[Q - Q_{db}]$ yields:

$$[Q - Q_{db}] = \frac{G_{d,old}}{G}[Q_{cal,old} - Q_o] \quad .$$

Then, substituting this into equation (8) leads to:

$$Q_{cal,new} = \frac{G}{G_{d,new}}\left[\frac{G_{d,old}}{G}(Q_{cal,old} - Q_o)\right] + Q_o \quad .$$

Simplifying, one obtains:

$$Q_{cal,new} = \frac{G_{d,old}}{G_{d,new}}(Q_{cal,old} - Q_o) + Q_o \quad . \qquad (9)$$

Finally, since the detector-to-detector differences have been removed in the original calibration process, there is no need to recalibrate on a detector-by-detector basis. G_d becomes the gain of the reference detector, G_{ref}. Two different approaches to determine G_{ref} are available to users. In the so-called CCRS method, G_{ref} is the gain of an individual reference detector. In the so-called NASA method, G_{ref} is calculated as $<G_d>$, where $<G_d>$ represents the mathematical average of G_d for the set of 16 detectors (32 detectors for band 8, the panchromatic band). Two different approaches will not be retained for the determination of the gain for recalibration for Landsat-7. Thus, $G_{d,new} = <G_{new}>$ and $G_{d,old} = G_{ref}$ and the recalibration equation becomes

$$Q_{cal,new} = \frac{G_{ref}}{<G_{new}>}(Q_{cal,old} - Q_o) + Q_o \qquad (10)$$

If the preference is to derive new estimates for L*, called L^*_{new}, from the original $Q_{cal,old}$ values, one can re-write equation (2), solving for L^*_{new}, as:

$$L^*_{new} = \frac{1}{G}(Q_{cal,new} - Q_o) . \qquad (11)$$

Then substitution of equation (7) for $Q_{cal,new}$ into equation (8) and simplifying yields:

$$L^*_{new} = \frac{1}{G}[\frac{G_{ref}}{< G_{new} >}(Q_{cal,old} - Q_o)] \quad . \qquad (12)$$

Formulation for TM Data

For Landsat TM data, the implementation took a slightly different approach compared to ETM+. The formalism presented here reflects these differences.

As in the case of ETM+, the data for TM are converted during processing from the original uncalibrated Q to calibrated Q_{cal}. The relative and absolute calibrations are combined into a single transformation of the form:

$$Q = \alpha_d Q_{cal} + \beta_d \qquad \text{, or} \qquad (13)$$

$$Q_{cal} = \frac{1}{\alpha_d}[Q - \beta_d] \qquad . \qquad (14)$$

Equation (14) is analogous to equation (3) in the general formulation. Q and Q_{cal} are the raw and calibrated signal levels (in counts), respectively. For TM data, the variable α_d , called the calibrated gain for detector d, has traditionally been used. This variable is equivalent to the ratio G/G_d in equation (3). The value of α_d is calculated for each scene by combining the relative gains of the individual detector elements obtained using scene statistics and the absolute gain of the reference detector, determined through an analysis of internal calibrator (IC) data from the scene being calibrated. In a manner very similar to the determination of α_d, the value of β_d is calculated for each scene by combining the relative biases of the individual detector elements obtained using scene statistics and the absolute bias of the reference detector, determined through an analysis of IC data from the scene being calibrated.

To recalibrate TM data, the relative (destriping) correction does not need to be undone, so all of the data have the radiometric calibration of the reference detector. To show this, equation (14) is re-written as:

$$Q_{cal} = \frac{1}{\alpha_{ref}}\left[Q - \beta_{ref}\right] \quad . \qquad (15)$$

For recalibration, the previously defined formalism expressed in equation (3) is used:

$$Q_{cal,new} = \frac{G}{G_{new}}[Q - Q_{db}] + Q_o \quad . \qquad (16)$$

In this case one is dealing with the calibration of the scene as a whole. The individual detector elements are no longer distinguished, so the subscript "d" has been dropped from the gain factor. It has been retained for one of the bias terms but, as will be shown, this bias term will cancel out of the formulation.

Solving equation (15) for Q yields, in the context of the original processing:

$$Q = \alpha_{ref}\, Q_{cal,old} + \beta_{ref} \quad . \qquad (17)$$

Substituting for Q in equation (8) leads to a recalibration equation for TM data:

$$Q_{cal,new} = \frac{G}{G_{new}}[\alpha_{ref} Q_{cal,old} + \beta_{ref} - Q_{db}] + Q_o \quad . \qquad (18)$$

The best estimate for Q_{db} is believed to be the line-by-line bias estimate made during the dark shutter observation at the end of each scan line in the "before-DC-restore" portion of the signal. These values are not recoverable in a recalibration context but they are nominally close to 3 digital counts. Thus, equation 18 simplifies to

$$Q_{cal,new} = \frac{G}{G_{new}}[\alpha_{ref} Q_{cal,old} + \beta_{ref} - 3] + Q_o \quad . \qquad (19)$$

If the preference is to derive new estimates for L*, called L^*_{new}, directly from the original $Q_{cal,old}$ values, one can re-write equation (2), solving for L^*_{new}, as:

$$L^*_{new} = \frac{1}{G}(Q_{cal,new} - Q_o) . \qquad (20)$$

Then substituting equation (19) for $Q_{cal,new}$ into equation (20) and simplifying yields:

$$L^*_{new} = \frac{1}{G_{new}}[\alpha_{ref} Q_{cal,old} + \beta_{ref} - 3]. \qquad (21)$$

In a small number of cases, users have collections of Level-0 TM data for which no radiometric processing was applied during product generation. Updated radiance data can be obtained in the solar-reflective bands for these data by combining equations (17) and (21), yielding:

$$L^*_{new} = \frac{1}{G_{new}}[Q - 3]. \qquad (22)$$

However, it should be noted that the resulting data will not be corrected for TM artefacts such as the memory effect and scan-correlated shifts, nor will they have been de-striped for relative detector gain differences.

Recalibration of TM Data without Knowledge of Radiometric Product Generation History

If a user has Landsat-5 TM data products for which there is no knowledge at all of the radiometric product generation history (i.e., no knowledge of α_{ref} and β_{ref}), the recalibration can be performed using the discrete band-averaged $<G_{new}>$ and $<G_{old}>$ derived from IC data from the Landsat-5 TM's lifetime. During Level-1 product generation, the NLAPS system records and archives a number of calibration parameters (rescaling gain and offset coefficients, as well as IC pulse height and location information for each lamp state, etc) in trending databases. This information is stored for all NLAPS products generated for the user community.

With this approach, lifetime $<G_{old}>$ and $<G_{new}>$ are supplied to the user community in the form of date-specific look-up tables. The $<G_{old}>$ are based on modeling data in the aforementioned trending databases as a function of time. The $<G_{new}>$ are obtained from the lifetime gain equations described earlier in this paper. However, it should be noted that this method does not produce the same accuracy as the use of known or obtainable α_{ref} and β_{ref} in the recalibration equations. Since the $<G_{old}>$ are obtained from a lifetime model, they provide an approximate gain for any given date, whereas α_{ref} and β_{ref} are the scene-specific radiometric processing coefficients that were originally applied during product generation. On occasions

when IC pulses could not be characterized successfully, NLAPS used prelaunch calibration coefficients as defaults to perform radiometric calibration. In these cases, there are no modeled data available.

Before and after recalibration, the recorded quantized signal level, Q (in counts), yields a pixel radiance of L^*_{old} and L^*_{new}, respectively, based on equation (1):

$$L^*_{old} = \frac{1}{< G_{old} >}(Q - Q_{db}) \quad , \qquad (23)$$

$$L^*_{new} = \frac{1}{< G_{new} >}(Q - Q_{db}) \quad . \qquad (24)$$

Thus, armed with $<G_{old}>$ and $<G_{new}>$ for the appropriate date, the user can update L^*_{old} to L^*_{new} as follows:

$$L^*_{new} = \left(L^*_{old}\right)\frac{< G_{old} >}{< G_{new} >} \quad . \qquad (25)$$